J. Fluid Mech. (1978), *vol.* 85, *part* 3, *pp.* 401–416
Printed in Great Britain

Radial source flow between parallel disks

By J. D. RAAL

Chemical Engineering Department, Queen's University,
Kingston, Ontario, Canada

(Received 1 July 1976 and in revised form 22 June 1977)

The vorticity transport equation is solved for radial incompressible flow between disks by a finite-difference method with discretization based on the method of Allen & Southwell. The solution permits detailed characterization of the flow for the Reynolds number range investigated, $1 \leqslant Re \leqslant 300$. Above $Re = 60$ separation is observed with the bubble size increasing rapidly with Re. The streamwise and transverse pressure and velocity gradients are examined to interpret the observed phenomena.

1. Introduction

Description of radial source flow between parallel disks, a problem with practical applications to centrifugal compressor diffusers and hydrostatic air bearings, has received considerable attention in the literature. The problem is of some intrinsic interest. For viscous flow the radial pressure distribution decreases logarithmically downstream whereas for ideal flow it is predicted to increase radially. In practice negative pressure gradients are usually found at small radii, changing to positive gradients further out. In the presence of wall friction the markedly adverse pressure gradient is sufficient, above a certain critical Reynolds number, to produce separation and reverse flow with reattachment further downstream. Turbulent flows may undergo a reverse transition to laminar flow, a phenomenon first noted by Kreith, Doughman & Kozlowski (1963).

Earlier approximate solutions of the problem by Osterle, Chou & Saibel (1957), Woolard (1957), Livesey (1960) and Moller (1963) were based on the Kármán momentum-integral method. As pointed out by Bird, Stewart & Lightfoot (1962, p. 114), however, the assumption of a fixed velocity profile leads to an inconsistency which may be significant (Savage 1964).

More recently Hunt & Torbe (1962), Jackson & Symmons (1965) and Savage (1964) used power-series expansions in the Navier–Stokes equations to solve for the velocity or pressure distributions with rather similar results. The co-ordinate expansion for the stream function used by Savage (1964) gave pressure distributions in good agreement, except at small radii, with the experimental results of Moller (1961). As pointed out by Wilson (1972) however, Savage's (1964) expansion does not apply in the region of small r (i.e. $r = O(Re^{\frac{1}{2}})$) and increasing the number of terms would give a worse prediction. In the region where inertia terms are important and the flow is shaped by inlet conditions the expansion would be invalid since the terms were evaluated with boundary conditions along the plate surface and plane of symmetry only. The agreement between theory and experiment was regarded as fortuitous (Wilson 1972).

Ishizawa (1965, 1966) in an extensive analysis combined a series expansion method for the inlet region with a momentum-integral method for the downstream region. He predicted no separation below $Re = 100$, a result contrary to that found in the present study. His separation point ($r_s = 1{\cdot}770$) for $Re = 100$ was close to that found in the present work ($r_s = 1{\cdot}794$) but the double vortex at $Re = 200$ found by Ishizawa was not confirmed here. Wilson (1972) points out that Ishizawa's analysis is based ultimately on the Schlichting (1934) model, which is considered incorrect through its failure to take into account the displacement effects of the boundary layers on the uniformity of the inviscid core. Further analyses of radial source flow were presented by Wilson (1971, 1972), who examined the influence of different entry conditions but found the problem to be mathematically intractable. Higgins (1975) formulated the radial source flow as a parameter perturbation problem to be analysed in the limit of high Reynolds numbers and suggested that difficulties of indeterminacy in earlier studies arose from attempts to match a co-ordinate expansion with a parameter expansion. The error in neglecting the third term of Savage's (1964) expansion was indicated to be $O(Re^{\frac{1}{2}}/r^2)^2$ and not $O(Re/r^2)^2$ as suggested by Wilson (1972). The critical Reynolds number for separation found by Higgins, $Re \geqslant 60$, is in essential agreement with the result of the more rigorous present study.

The series expansion for the stream function used by Patrat (1975) gave pressure distributions in good agreement with experimental values ($Re > 12000$) except at small radii. The disagreement at small radii is to be expected since no initial (upstream) conditions were applied.

In the present study the author presents results obtained from a finite-difference solution of the full Navier–Stokes equations with a discretization procedure based on the method of Allen & Southwell (1955). In accordance with expectation the latter procedure conferred remarkable stability on the computations and permitted the use of over-relaxation to accelerate convergence. The solution was obtained in the form of stream-function and vorticity distributions, from which velocity and pressure distributions may readily be calculated. Our results indicated that for $Re \leqslant 60$ there is no separation, that the separation point moves upstream with increasing Re and that the length of the separation bubble increases rapidly with Re. The absence of separation for $Re \leqslant 60$ is surprising in view of the still strongly adverse pressure gradient along the wall but can be interpreted by examining the transverse pressure gradient, which attains a substantial magnitude in the region near the wall at low Reynolds number. Computation of transverse velocity and pressure distributions defined the region in which boundary-layer simplifications are invalid.

2. The governing equations

For radial axisymmetric flow of a constant-property fluid between large disks the governing equation in terms of the stream function ψ is

$$\left\{\frac{\partial\psi}{\partial Z}\left(\frac{\partial}{\partial r}-\frac{1}{r}\right)-\left(\frac{\partial\psi}{\partial r}+\frac{\psi}{r}\right)\frac{\partial}{\partial Z}\right\}\nabla^2\psi=\frac{1}{Re}\nabla^2(\nabla^2\psi). \tag{2.1}$$

The variables in the above equation have been rendered dimensionless through the transformations

$$r=\bar{r}/\bar{h},\quad Z=\bar{Z}/\bar{h},\quad \psi=4\pi\bar{h}\bar{\psi}/\bar{Q}.$$

The barred quantities are dimensional. The Reynolds number is defined as $Re = \bar{Q}/4\pi\bar{\nu}\bar{h}$ with $\bar{Q}$ the volumetric flow rate and $2\bar{h}$ the gap between the plates, which lie in the planes $\bar{Z} = \pm\bar{h}$.

Introducing the vorticity

$$\omega = \nabla^2\psi = \frac{\partial^2\psi}{\partial Z^2} + \frac{\partial^2\psi}{\partial r^2} + \frac{1}{r}\frac{\partial\psi}{\partial r} - \frac{\psi}{r^2}, \tag{2.2}$$

(2.1) becomes

$$\frac{\partial\psi}{\partial Z}\left(\frac{\partial\omega}{\partial r} - \frac{\omega}{r}\right) - \left(\frac{\partial\psi}{\partial r} + \frac{\psi}{r}\right)\frac{\partial\omega}{\partial Z} = \frac{1}{Re}\nabla^2\omega. \tag{2.3}$$

To reduce the region of computation the transformation

$$\eta = 1 - 1/r \tag{2.4}$$

was used. This compresses the scale in terms of the radial co-ordinate r at large values of r, a region where gradients are mild. Equations (2.2) and (2.3) become

$$(1-\eta)^2\frac{\partial\psi}{\partial Z}\frac{\partial\omega}{\partial\eta} - (1-\eta)^2\frac{\partial\psi}{\partial\eta}\frac{\partial\omega}{\partial Z} - \omega(1-\eta)\frac{\partial\psi}{\partial Z} - \psi(1-\eta)\frac{\partial\omega}{\partial Z}$$
$$= \frac{1}{Re}\left\{\frac{\partial^2\omega}{\partial Z^2} + (1-\eta)^4\frac{\partial^2\omega}{\partial\eta^2} - (1-\eta)^3\frac{\partial\omega}{\partial\eta} - \omega(1-\eta)^2\right\}, \tag{2.5}$$

$$\omega = \frac{\partial^2\psi}{\partial Z^2} + (1-\eta)^4\frac{\partial^2\psi}{\partial\eta^2} - (1-\eta)^3\frac{\partial\psi}{\partial\eta} - (1-\eta)^2\psi. \tag{2.6}$$

The above equations may be formulated alternatively in terms of $\psi' = \psi r$ by noting that in general ψ and the streamwise velocity U are proportional to r^{-1}. Both ψ' and ψ satisfy the continuity equation but only lines of constant ψ' are tangential to the vector velocity. The stream-function plots shown later are for ψ' since the latter is physically more meaningful.

3. Boundary conditions

Equations (2.5) and (2.6) were solved for two different inlet conditions. For case I uniform approach flow with zero vorticity at the plate entrance ($r = 1$) was assumed, giving

$$\eta = 0, \quad \omega = 0, \quad \psi = Z. \tag{3.1}$$

For case II the physically more realistic model of flow towards an infinite cascade of parallel plates (Wilson 1971) was assumed with uniform irrotational flow at some plane $r = r_0$ ($\eta = \eta_0$) upstream from the entrance, i.e.

$$\eta = \eta_0, \quad \omega = 0, \quad \psi = Z/r_0 = Z(1-\eta_0). \tag{3.2}$$

It should be noted that (3.2) permits diffusion of vorticity upstream from the entrance to the plates. Values of r_0 sufficiently small to permit unrestricted vorticity diffusion are easily found by examining vorticity distributions obtained in the solutions for the region $r_0 < r < 1$. In practice $r_0 \geqslant 0{\cdot}667$ was found satisfactory for all Reynolds numbers greater than unity studied.

At large distances downstream the flow assumes the fully developed parabolic profile for all Re:

$$\eta = \eta_\infty, \quad \omega = -3Z(1-\eta), \quad \psi = \tfrac{3}{2}(1-\eta)(Z - \tfrac{1}{3}Z^3). \tag{3.3}$$

Along the plane of symmetry between the plates,

$$\psi = 0 = \omega \quad \text{on} \quad Z = 0. \tag{3.4}$$

Along the solid surface (for $\eta \geqslant 0$) the no-slip condition is enforced, with

$$\omega = \nabla^2\psi, \quad \psi = (1-\eta) \quad \text{on} \quad Z = 1. \tag{3.5a,b}$$

The surface vorticity is unknown but is evaluated from interior values of ψ and ω after each iteration using a finite-difference form of (3.5a). This is developed in the appendix using a modification of Wood's (1954) method.

For case II, ψ and ω must further be specified in the fluid plane $Z = 1$ ahead of the solid surface. From symmetry considerations,

$$\omega = 0, \quad \psi = 1-\eta \quad \text{on} \quad Z = 1, \quad \eta_0 < \eta < 0. \tag{3.6}$$

4. Discretization and numerical solution

Successful numerical solutions were obtained using several different discretization and co-ordinate transformation schemes. These included using

(a) central differences for all derivatives with the governing equations in terms of Z and r,

(b) central differences for all derivatives and transformed co-ordinates according to $Z = 1-(1-x)^2$ and $\eta = 1-1/r$,

(c) Allen & Southwell's (1955) 'latent exponentials' discretization scheme for (2.5) and central differences for the derivatives in (2.6).

With both scheme (a) and scheme (b) above stability problems were encountered at the higher Reynolds numbers, necessitating the use of very small relaxation factors (see (4.1) below) and leading to long computation times. Transformation of the Z co-ordinate in scheme (b) was attractive since a very fine Z spacing was produced near the solid surface (where vorticity gradients are steep) when fixed increments in x were taken. The excellent stability conferred on the computations by Allen & Southwell's discretization scheme led to the adoption of scheme (c), i.e. (2.5) and (2.6) were solved subject to the boundary conditions given in (3.3)–(3.5) together with equation (3.1) (scheme I) or (3.2) and (3.6) (scheme II). In their original paper Allen & Southwell (1955) presented no physical arguments to justify the approximations used in the vorticity transport equation to derive a finite-difference algorithm for the vorticity. It is evident however that their method assumes in essence that the vorticity flux is constant over a small interval for either of the two co-ordinate directions. For the co-ordinate normal to a solid boundary, at least, this is reasonable since the total vorticity transport is more nearly constant than that due to convection or diffusion alone. The method leads to an exponential representation of the vorticity (e.g. equation (A 4) in the appendix). This is a more flexible and perhaps more accurate form, particularly near a solid boundary, than the Taylor expansions on which conventional central-difference formulae are based. Details of the development are given in the appendix.

The equations were solved by a point-iteration scheme employing Liebman's procedure, with a suitable arbitrary initial distribution for ψ and ω. Convergence was accelerated by using relaxation factors, e.g. for the vorticity

$$\omega^{n+1} = \omega^n + W(\omega^{n+1} - \omega^n), \tag{4.1}$$

Re	Step sizes $A(=\Delta\eta)$	Step sizes $B(=\Delta Z)$	Inner and outer computational radii r_0	Inner and outer computational radii r_∞	Number of mesh points	Number of iterations for convergence
1	0·05	0·0667	0·6667	20·0	480	229
1	0·061	0·0667	0·5577	41·67	480	244
30	0·08125	0·10	0·6375	40·0	220	173
30	0·05	0·0667	0·6667	20·0	480	334
60	0·08	0·10	0·6410	25·0	220	214
60	0·05	0·0667	0·6667	20·0	480	450
75	0·05	0·0667	0·6667	20·0	480	393
100	0·05	0·0667	0·6667	20·0	480	467
100	0·0465	0·0667	0·5444	42·55	640	580
200	0·0465	0·0667	0·7289	42·55	480	700
300	0·05	0·0667	0·6667	20·0	480	1200†

† Vorticity not fully converged.

TABLE 1. Computational parameters.

where W is the relaxation factor and n symbolizes the nth iteration. Since optimum numerical values for W cannot be satisfactorily predicted the latter were found empirically by trial and error. The author's experience was similar to that of Wang & Longwell (1964), viz. that over-relaxation (e.g. $W = 1{\cdot}2$) should be used in the initial stages followed by a reduction in W to a value less than unity (e.g. $W = 0{\cdot}8$) as the iteration proceeds. The rate of convergence was primarily dependent on the value of W for the vorticity calculation.

5. Step size and convergence criterion

Details of step sizes, inner and outer boundary locations (r_0, r_∞) and the number of iterations required for convergence are given in table 1. Step sizes were chosen sufficiently small that a further reduction had a negligible influence on the computed results. The leading edge of the plate ($r = 1$, $Z = 1$) is a discontinuity and there is some uncertainty about the computed quantities in the immediate vicinity of this point. The discontinuity could be removed by specifying the geometry and radius of curvature of the leading edge. This would increase considerably the complexity of the computational problem and does not seem worthwhile.

Solutions were considered to have converged when at all mesh points

$$\left|\frac{\psi^{n+1}-\psi^n}{\psi^n}\right| < 10^{-4}, \quad \left|\frac{\omega^{n+1}-\omega^n}{\omega^n}\right| < 10^{-4}, \tag{5.1}$$

6. Computation of pressure and velocity distributions

Streamwise and transverse velocities are readily computed from their respective definitions:

$$U = \partial\psi/\partial Z, \tag{6.1}$$

$$V = -\partial\psi/\partial r - \psi/r = -(1-\eta)^2\,\partial\psi/\partial\eta - \psi(1-\eta). \tag{6.2}$$

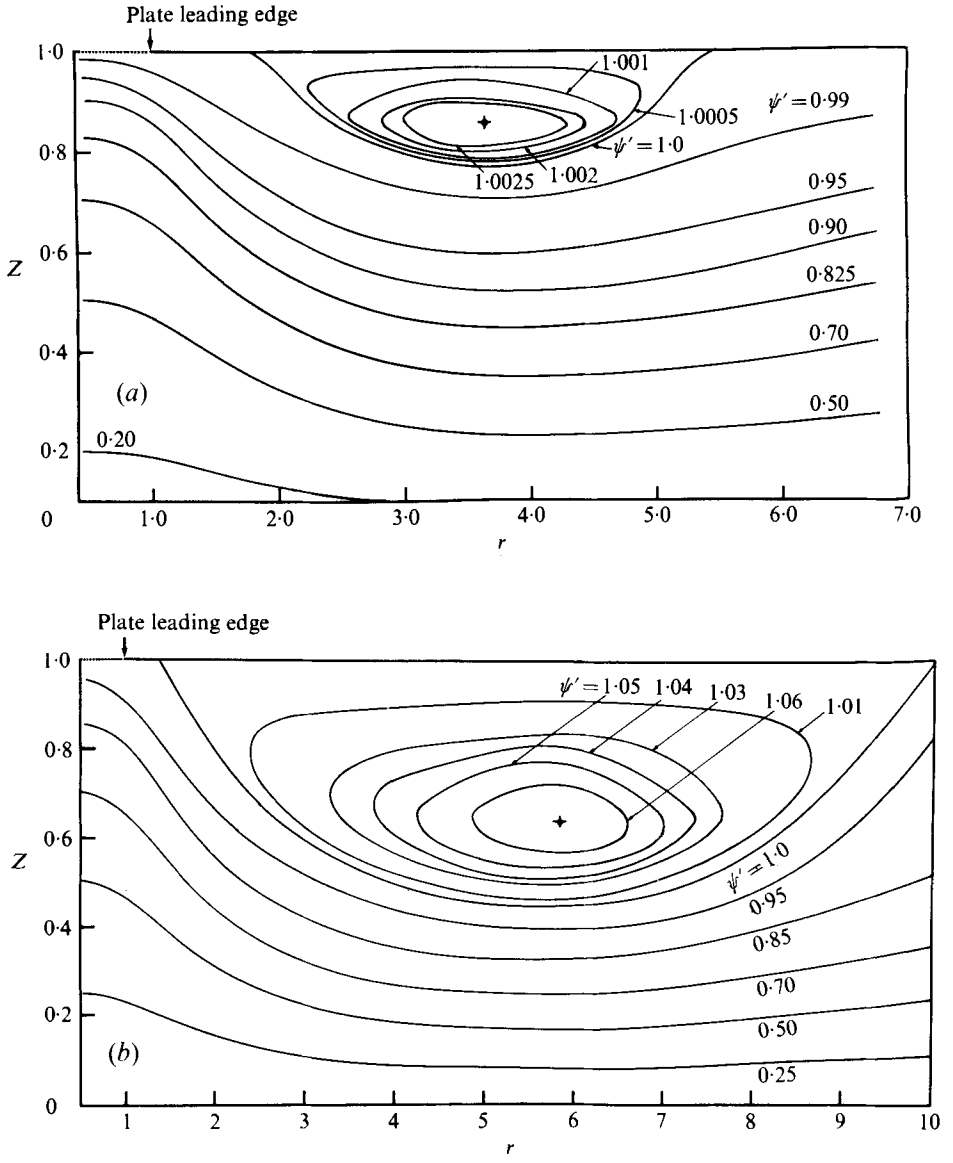

FIGURE 1. Streamline pattern for flow at (*a*) $Re = 100$ and (*b*) $Re = 200$.

By integration of one component of the Navier–Stokes equations in cylindrical co-ordinates the following equation for the radial pressure distribution on the plane $Z = 1$ is obtained:

$$P_s(\eta) - P_0 = U_0^2 - U^2 + \frac{2}{Re}(1-\eta)^3 \frac{\partial}{\partial \eta}\left(\frac{U}{1-\eta}\right) + \frac{2}{Re}\int_{\eta_0}^{\eta} \frac{\partial \omega / \partial Z}{(1-\eta)^2} d\eta. \tag{6.3}$$

For the region $\eta \geqslant 0$ only the last term in (6.3) is non-zero. P is the dimensionless pressure coefficient $p/\frac{1}{2}\rho U_0^2$, the subscript s denotes the plane $Z = 1$ and the subscript 0 denotes the plane $r = r_0$.

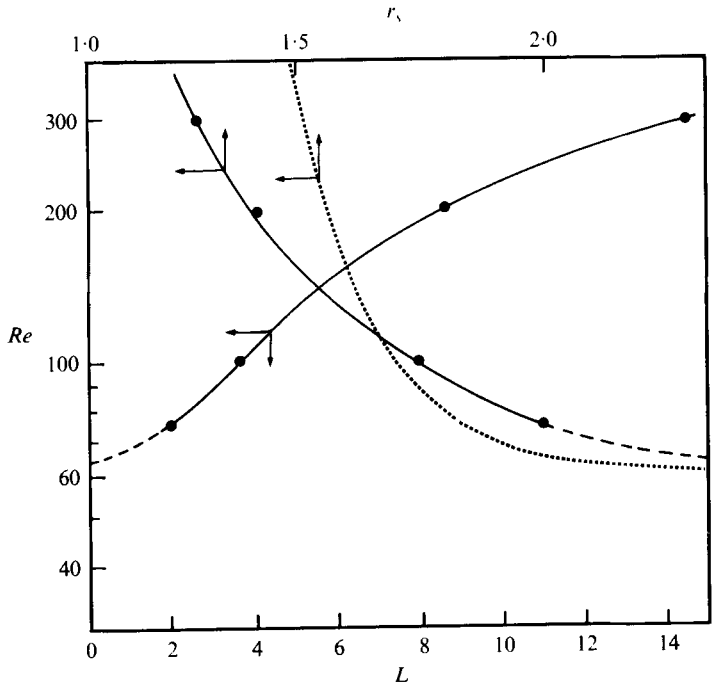

FIGURE 2. Vortex length L and separation point r_s as a function of Reynolds number. The dotted curve is the separation point predicted by Higgins (1975).

Transverse pressure distributions were also computed for the region near the plate leading edge ($\eta = 0$) using the equation

$$P(Z) - P_s(\eta) = 2(1-\eta)^2 \int_Z^1 \left\{ \frac{(1-\eta)}{Re} \frac{\partial}{\partial \eta} \left(\frac{\omega}{1-\eta} \right) + U \frac{\partial V}{\partial \eta} \right\} dZ - V^2(Z). \tag{6.4}$$

Equations (6.3) and (6.4) are exact. The integrals were evaluated using Simpson's rule.

7. Computed results and discussion

The adequacy of the downstream computational boundary r_∞ was tested for Reynolds numbers of 30 and 100 by increasing the value of r_∞ from 20 to 40 and 42·55 respectively. This gave no significant change in the computed results. Figures 1(a) and (b) show streamline plots for $Re = 100$ and 200 for case II, i.e. with upstream diffusion of vorticity permitted. The rapid increase in bubble size with Reynolds number is evident and is also shown in figure 2, where the vortex length and the separation point r_s are plotted as functions of Re. The separation point is defined here as the point at which the vorticity changes sign. Figure 2 suggests $Re = 64$ as the critical Reynolds number for separation to occur, a value much lower than that proposed by Ishizawa (1966) ($Re = 100$). The vortex depicted in figure 1(b) differs substantially from that found by Ishizawa (1966). The discrepancies may be due in part to the convergence problems for Ishizawa's series solution. Also shown in figure 2 is the separation point predicted by Higgins (1975). The divergence of this prediction from that of the present study may arise from approximations near the leading edge

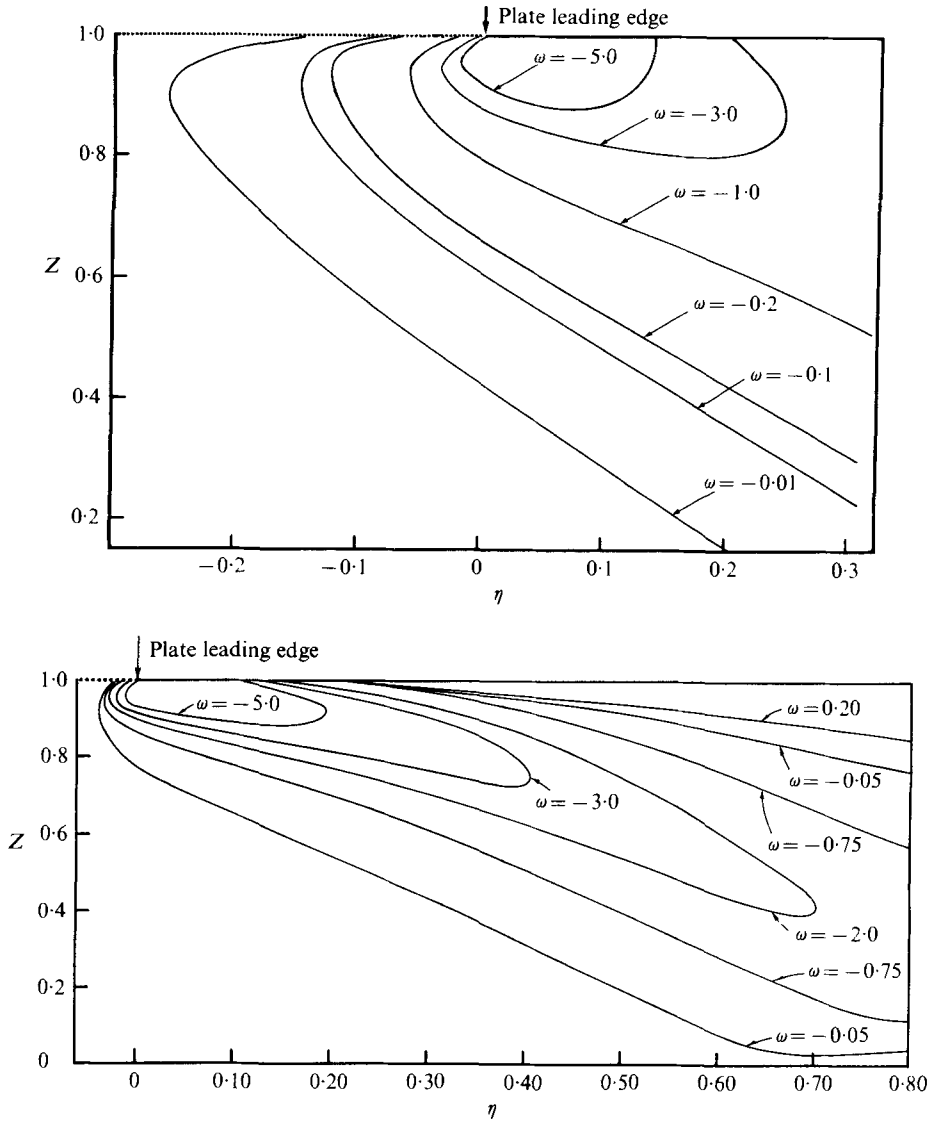

FIGURE 3. Lines of constant vorticity for flow at (*a*) $Re = 30$ and (*b*) $Re = 300$; case II.

in the boundary-layer and inviscid-core regions of the Higgins model. The computations were insensitive to the position r_0 of the upstream computational boundary provided that r_0 was sufficiently small. A reduction in r_0 from 0·667 to 0·544 for $Re = 100$, for example, did not change the stream-function or the vorticity distributions. It is interesting to note that when the more restrictive boundary condition (3.1) was used (i.e. uniform approach flow with zero vorticity at $\eta = 0$, case I) vortex formation was found for $Re = 60$.

The lines of constant vorticity in figures 3(*a*) and (*b*) illustrate the significant vorticity diffusion upstream in the region of low velocity and its convection downstream further from the surface.

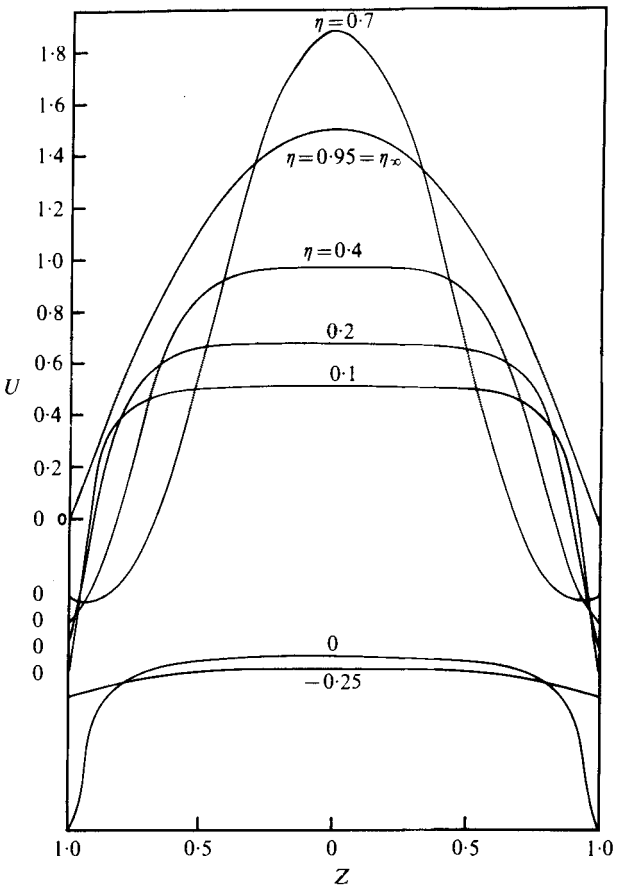

FIGURE 4. Profiles of radial velocity U for $Re = 100$.

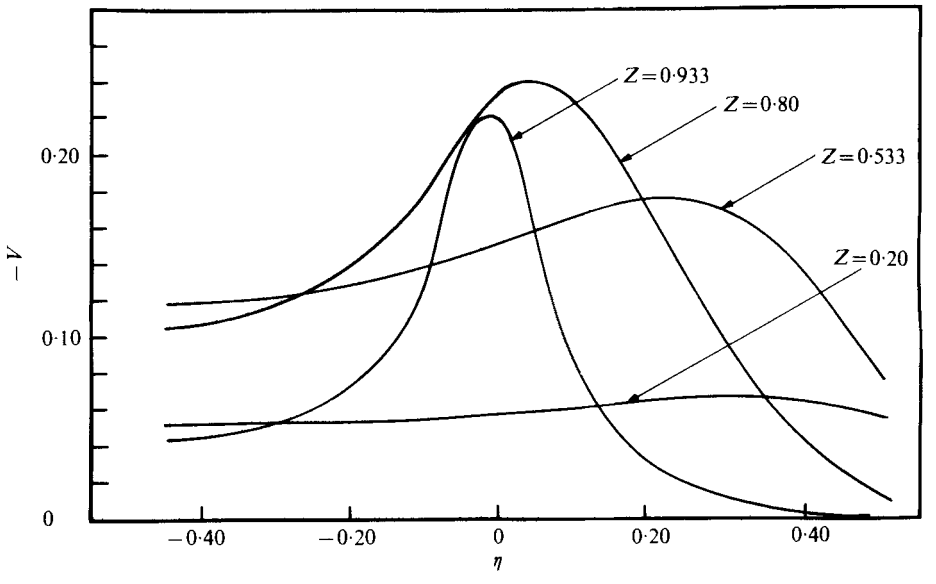

FIGURE 5. Profiles of transverse velocity V as a function of radial distance at various fluid planes Z for $Re = 100$.

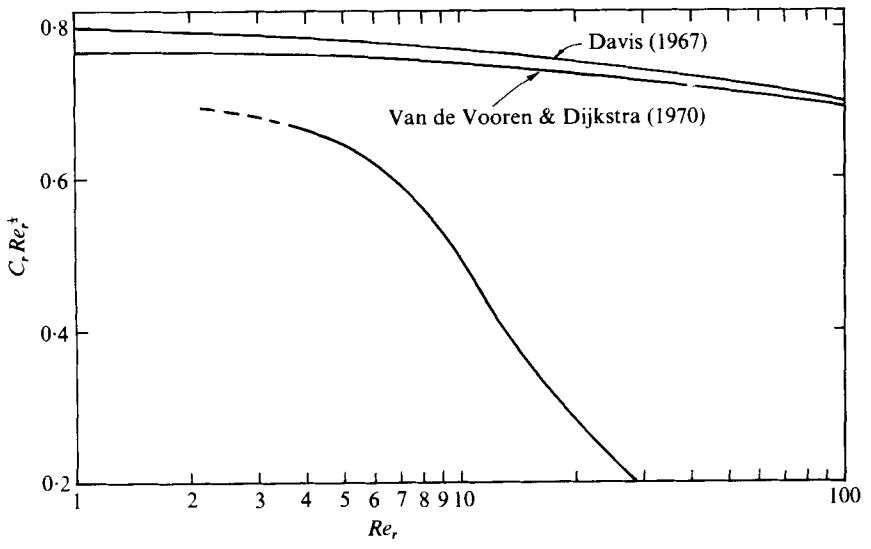

FIGURE 6. Local drag-coefficient product as a function of local Reynolds number, computed from the solution for $Re = 100$.

r	$C = \frac{1{\cdot}3282}{16}\left(\frac{Re}{r-1}\right)^{\frac{1}{2}}$ (boundary-layer theory)	$C = \frac{-V}{(1-z)^2}$ (V from numerical solutions)
1·0	Leading edge	
1·303	4·98	5·24
1·387	3·45	3·47
1·483	2·48	2·28
1·794	Separation point	

TABLE 2. Comparison of boundary-layer prediction $V = -Cy^2$ with solutions for transverse velocity near $y = 0$ for $Re = 100$.

Radial velocity profiles are shown in figure 4 for $Re = 100$. The non-uniform profile upstream of the plate entrance (e.g. at $\eta = -0{\cdot}25$) and at the entrance ($\eta = 0$), reflecting upstream diffusion of vorticity, may be noted. Although not discernible in the diagram, there is a small concavity in the profiles near $\eta = 0{\cdot}4$ similar to that found by Wang & Longwell (1964) for non-radial flow. This phenomenon, usually associated with instability, was observed for all $Re \geqslant 75$. The extent of the concavity was approximately the same at all Re but its location moved downstream with Re. The small region of reverse flow near the wall is evident.

Transverse velocity profiles are shown in figure 5 for $Re = 100$. The substantial magnitude of the velocity near the wall in the inlet region confirms the inapplicability of boundary-layer theory for this Reynolds number. Even at $Re = 300$ the transverse velocity remains appreciable in the inlet region. Similarly significant transverse velocities were found by Wang & Longwell (1964) for flow in the inlet section of parallel plates, suggesting a comparison with other solutions in the literature for flow near the leading edge of a flat plate. In figure 6 the product $C_r Re_r^{\frac{1}{2}}$ [C_r = local drag

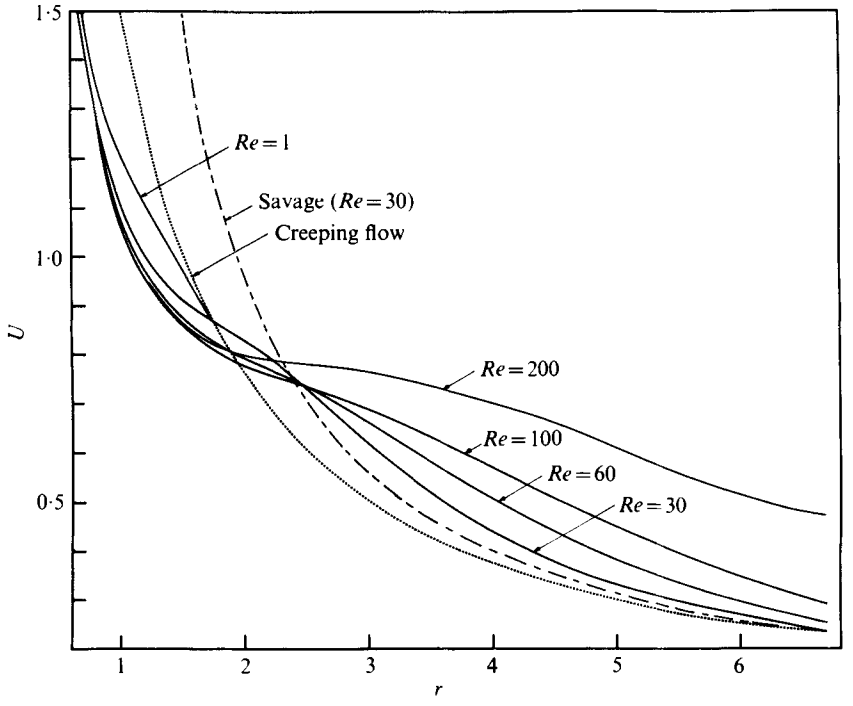

FIGURE 7. Comparison of centre-line velocities with the prediction of viscous flow and that of Savage (1964).

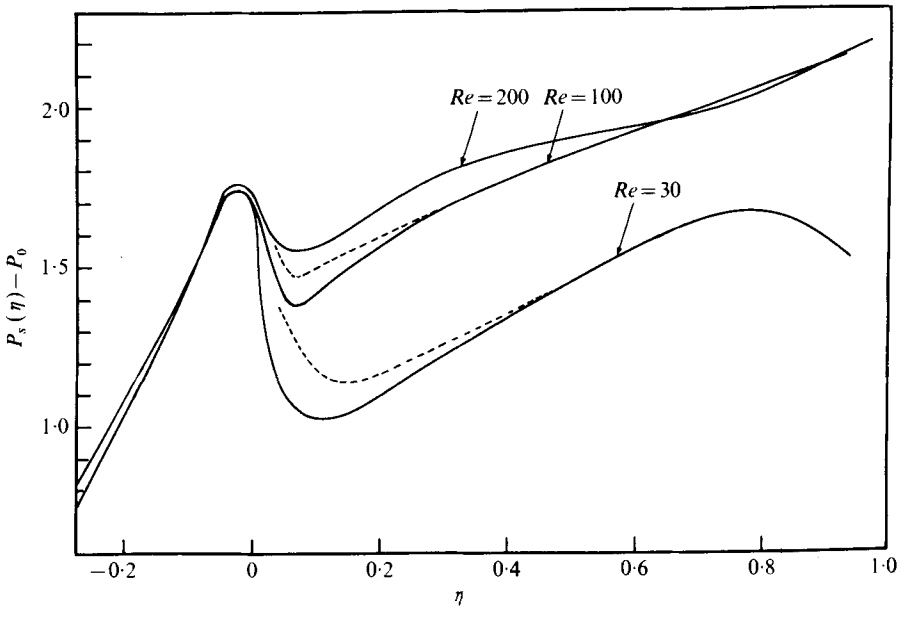

FIGURE 8. Dimensionless pressure coefficients along the planes $Z = 1$ (solid lines) and $Z = 0{\cdot}95$ (dashed lines).

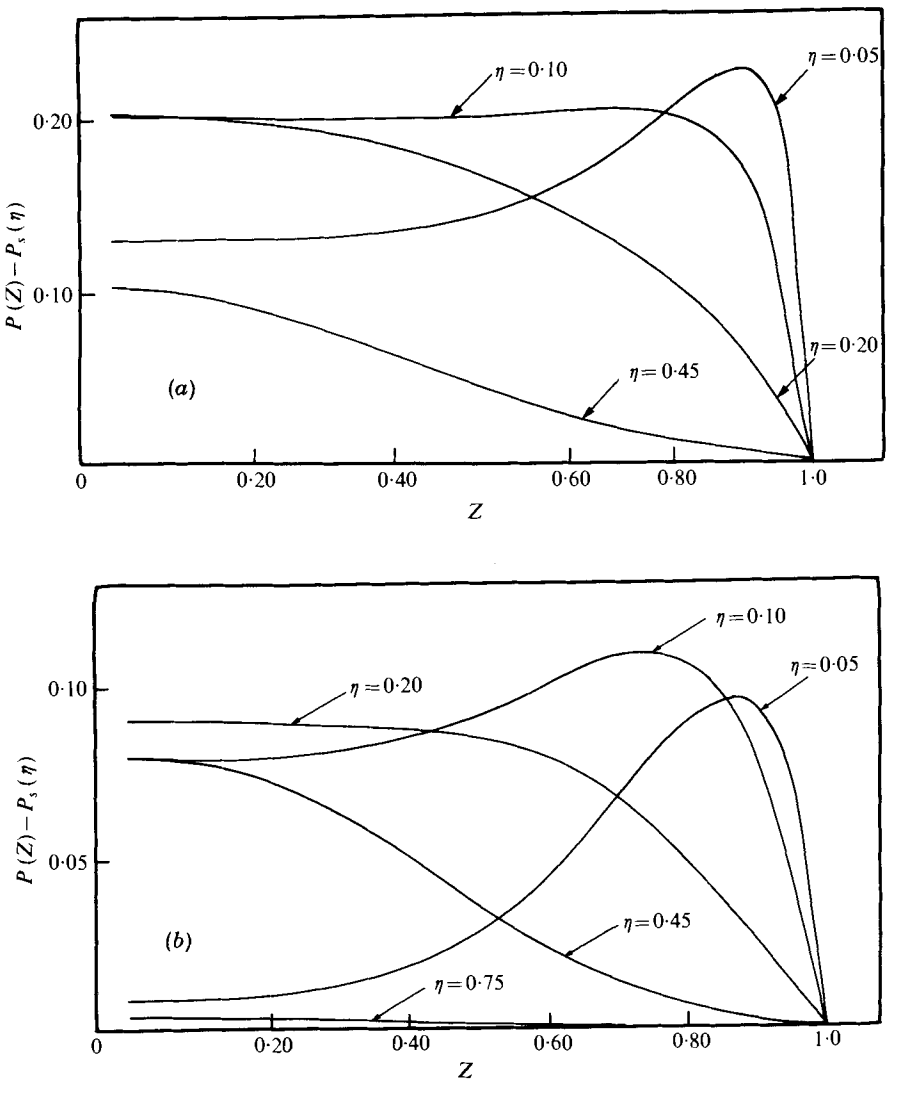

FIGURE 9. Transverse pressure distributions at various radial distances for (*a*) $Re = 30$ and (*b*) $Re = 100$.

coefficient, Re_r = local Reynolds number = $Re(r-1)$] is compared with predictions from the series-truncation method of Davis (1967) and that of Van de Vooren & Dijkstra (1970), who matched Carrier & Lin's (1948) leading-edge solution with a downstream boundary-layer solution. Although the physical situations are not directly comparable owing to the radial nature of the flow in the present study, the drag-coefficient product approaches a value comparable to those of the literature predictions as $\eta \to 0$, as expected.

For a region between the leading edge ($\eta = 0$) and the separation point ($\eta = \eta_s$) classical boundary-layer theory gives a valid approximation to the flow near the surface. This may be seen from table 2, where the boundary-layer prediction for the transverse velocity $V = -cy^2$ ($c = f(\eta) \neq f(y)$ near $y = 0$) is compared with results

from the present numerical solution for $Re = 100$. The two predictions are in close agreement near the midpoint between the leading edge and the separation point.

Centre-line velocities are depicted in figure 7 for several Reynolds numbers. For $Re > 1$ the profiles depart substantially from the viscous-flow parabolic profile and show points of inflexion near the entrance owing to boundary-layer development. The equation developed by Savage (1964) is plotted for $Re = 30$ and his prediction is seen to depart substantially from that of the present work in the region of small r. Centre-line velocities for case I (no vorticity diffusion upstream) were substantially larger than for case II.

Pressure coefficients along the plane $Z = 1$, normalized with respect to the pressure P_0 at $r = r_0 = 0{\cdot}6667$, are shown for Reynolds numbers of 30, 100 and 200 in figure 8. A strongly adverse pressure gradient develops along the wall near the inlet even at low Re. The surprising absence of separation at, for example, $Re = 60$ may be attributed to the modification of the radial surface pressure gradient in the wall region by acceleration effects due to the growing boundary layers. As shown in figures 9(*a*) and (*b*), transverse pressure gradients in the wall region become very large at small η, particularly for low Reynolds numbers, and rapidly decrease downstream. This leads to the modified radial pressure distributions shown as dotted lines above the solid curves of figure 8 for the plane $Z = 0{\cdot}95$, i.e. close to the solid surface. This reduction in the adverse radial pressure gradient is presumably sufficient to prevent reverse flow in this region for $Re \leqslant 60$. It is evident from figures 9(*a*) and (*b*) that the external pressure profile is not 'impressed' on the boundary layer in the entrance region. The criterion for separation proposed in Schlichting's (1960, p. 261) boundary-layer approach,

$$\sigma = U_e U_e''/(U_e')^2 < 11 \quad (U_e = \text{free-stream velocity}),$$

gave incorrect predictions for the Reynolds numbers studied.

The experimental pressure profiles published by Moller (1963), Jackson & Symmons (1965) and Morgan & Saunders (1960) were obtained for $Re > 19000$ and cannot be directly compared with those of the present study.

8. Conclusion

Steady-state solutions of the full vorticity transport equation have been obtained for two different entrance conditions. The appreciable diffusion of vorticity upstream found in case II confirms that its curtailment in case I is not realistic, particularly at low Reynolds numbers. The latter boundary condition should be abandoned in similar future computations.

The excellent stability conferred on the vorticity computations by Allen & Southwell's discretization procedure permitted the use of over-relaxation and gave more rapid convergence than conventional finite-difference schemes. A much broader trial of their procedure than is at present evident in the literature seems warranted. The instabilities experienced with the central-difference discretization procedure could arise merely from the numerics of computation (as found, for example, by Van de Vooren & Dijkstra (1970) for flow over a flat plate) or may reflect instability in the real flow as in flow over a cylinder for $Re > 40$ (when vortex shedding occurs). The observed concavity in the velocity profiles lends credence to the latter speculation. Steady-state computations for flows with vortex shedding, if carefully performed,

still give results, e.g. drag coefficients, in close agreement with the best experimental results. The question of flow stability remains to be answered by experiment or by a time-dependent study such as that of Thoman & Szewczyk (1969).

The author wishes to thank Dr D. J. Van der Merwe for suggesting the problem and for helpful suggestions during the course of the work, which was performed at the University of the Witwatersrand, Johannesburg, during sabbatical leave in 1975–6.

Appendix. Finite-difference form of the vorticity transport equation

Equation (2.5) is arranged in the form

$$\left\{\frac{\partial^2\omega}{\partial Z^2}+\kappa\frac{\partial\omega}{\partial Z}-\alpha\omega\right\}+(1-\eta)^4\left\{\frac{\partial^2\omega}{\partial\eta^2}+\lambda\frac{\partial\omega}{\partial\eta}-\beta\omega\right\}=0, \tag{A 1}$$

i.e.
$$A+(1-\eta)^4B=0,$$

with
$$\kappa = Re(1-\eta)\left\{\psi+(1-\eta)\frac{\partial\psi}{\partial\eta}\right\},$$

$$\lambda = -\frac{1}{1-\eta}-\frac{Re}{(1-\eta)^2}\frac{\partial\psi}{\partial Z},$$

$$\alpha = (1-\eta)^2,$$

$$\beta = -\frac{1}{(1-\eta)^3}Re\frac{\partial\psi}{\partial Z}.$$

Following Allen & Southwell (1955), assuming A, κ, α = constant gives

$$\frac{\partial^2\omega}{\partial Z^2}+\kappa\frac{\partial\omega}{\partial Z}-\alpha\omega = A, \tag{A 2}$$

while assuming B, λ, β = constant gives

$$\frac{\partial^2\omega}{\partial\eta^2}+\lambda\frac{\partial\omega}{\partial\eta}-\beta\omega = B. \tag{A 3}$$

The solution of (A 2) is
$$\omega = He^{\delta Z}+Ge^{\mu Z}-A/\alpha, \tag{A 4}$$

with δ and μ the roots of the homogeneous part of (A 2). Referring to the mesh points shown in figure 10, (A 4) may be written for points B, E and D. Elimination of the constants H and G from the three resulting equations produces an expression for the remaining constant A in terms of the vorticity at points B, E and D:

$$A_E = \frac{\alpha\{(\omega_E e^{\mu b}-\omega_B)e^{-\delta b}+\omega_E-\omega_D e^{\mu b}\}}{(1-e^{\mu b})(e^{-\delta b}-1)}. \tag{A 5}$$

A similar procedure for (A 3) gives

$$B_E = \frac{\beta\{(\omega_E e^{\epsilon a}-\omega_A)e^{-\gamma a}+\omega_E-\omega_c e^{\epsilon a}\}}{(1-e^{\epsilon a})(e^{-\gamma a}-1)}, \tag{A 6}$$

with ϵ and γ the roots of the homogeneous part of (A 3). In the above equations a and b are the step sizes $\Delta\eta$ and ΔZ respectively.

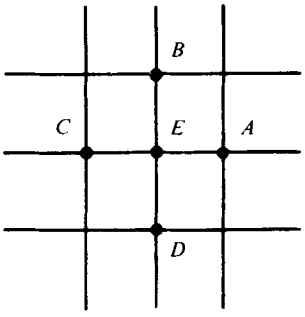

FIGURE 10

Substitution of the above expressions for A and B in (A 1) gives, finally,

$$\omega_E C_E = \omega_A C_A + \omega_B C_B + \omega_C C_C + \omega_D C_D \tag{A 7}$$

with

$$C_A = (1-\eta)^4 \beta_E e^{-\gamma a}/(1-e^{\epsilon a})(e^{-\gamma a}-1),$$
$$C_B = \alpha_E e^{-\delta b}/(1-e^{\mu b})(e^{-\delta b}-1),$$
$$C_D = \alpha_E e^{\mu b}/(1-e^{\mu b})(e^{-\delta b}-1),$$
$$C_C = (1-\eta)^4 \beta_E e^{\epsilon a}/(1-e^{\epsilon a})(e^{-\gamma a}-1),$$
$$C_E = C_B e^{\mu b} + C_D e^{-\mu b} + C_A e^{\epsilon a} + C_C e^{-\epsilon a}.$$

The stream-function derivatives appearing in the definitions of κ, λ and β above were discretized using central-difference formulae. The roots δ and μ are given by

$$\delta = \tfrac{1}{2}[-\kappa + (\kappa^2+4\alpha)^{\frac{1}{2}}], \quad \mu = \tfrac{1}{2}[-\kappa - (\kappa^2+4\alpha)^{\frac{1}{2}}].$$

Corresponding expressions hold for γ and ϵ respectively with λ and β replacing κ and α.

Vorticities were computed from (A 7) and stream-function values were computed from (2.6) written in finite-difference form using central differences for all derivatives.

Surface vorticity. Let S denote the solid surface and $S+1$ the next interior point. Expansion of the stream function about the point S yields at any given radial position i

$$\psi_{i,S+1} = \psi_{i,S} + \left(\frac{\partial \psi}{\partial x}\right)_{i,S} \Delta x + \frac{1}{2}\left(\frac{\partial^2 \psi}{\partial x^2}\right)_{i,S} (\Delta x)^2 + \frac{1}{6}\left(\frac{\partial^3 \psi}{\partial x^3}\right)_{i,S} (\Delta x)^3. \tag{A 8}$$

For convenience the co-ordinate x $(=1-Z)$ is used.

No slip requires that $U = 0 = \partial\psi/\partial x$ in (A 8). Also, it is easily shown that

$$\left(\frac{\partial \omega}{\partial Z}\right)_{i,S} = \frac{\partial}{\partial Z}\left(\frac{\partial U}{\partial Z} - \frac{\partial V}{\partial r}\right) = \left(\frac{\partial^3 \psi}{\partial Z^3}\right)_{i,S} \tag{A 9}$$

by enforcing $U = 0$ for all $r > 1{\cdot}0$. Substitution of these expressions in (A 8) gives

$$\psi_{i,S+1} = \psi_{i,S} + \tfrac{1}{2}B^2 \omega_{i,S} + \tfrac{1}{6}B^3 (\partial\omega/\partial x)_{i,S} \tag{A 10}$$

(B = step size ΔZ). Equation (A 10) is discretized further using a more accurate forward-difference formula for $\partial\omega/\partial x$ $(=-\partial\omega/\partial Z)$ than that used by Wood (1954) in a similar derivation. Substitution of $\partial\omega/\partial x = (-3\omega_{i,S} + 4\omega_{i,S+1} - \omega_{i,S+2})/2B$ and solving for $\omega_{i,S}$ gives, finally,

$$\omega_{i,S} = 4(\psi_{i,S+1} - \psi_{i,S})/B^2 - \tfrac{1}{3}(4\omega_{i,S+1} - \omega_{i,S+2}). \tag{A 11}$$

Equation (A 11) is used to compute surface vorticities in the iterative procedure.

REFERENCES

ALLEN, D. N. DE G. & SOUTHWELL, R. V. 1955 *Quart. J. Mech. Appl. Math.* **8**, 129.
BIRD, R. B., STEWART, W. E. & LIGHTFOOT, E. N. 1960 *Transport Phenomena.* Wiley.
CARRIER, G. F. & LIN, C. C. 1948 *Quart. Appl. Math.* **6**, 63.
DAVIS, R. T. 1967 *J. Fluid Mech.* **27**, 691.
HIGGINS, B. G. 1975 M.Sc. thesis, University of Witwatersrand, Johannesburg.
HUNT, J. B. & TORBE, I. 1962 *Int. J. Mech. Sci.* **4**, 503.
ISHIZAWA, S. 1965 *Japan Soc. Mech. Engrs* **8**, 353.
ISHIZAWA, S. 1966 *Japan Soc. Mech. Engrs* **9**, 86.
JACKSON, J. D. & SYMMONS, G. R. 1965 *Appl. Sci. Res.* **15**, 59.
KREITH, F., DOUGHMAN, E. & KOZLOWSKI, H. 1963 *Trans. A.S.M.E.* C **85**, 153.
LIVESEY, J. L. 1960 *Int. J. Mech. Sci.* **1**, 84.
MOLLER, P. S. 1963 *Aero. Quart.* **14**, 163.
MORGAN, D. G. & SAUNDERS, A. 1960 *Int. J. Mech. Sci.* **2**, 8.
OSTERLE, J. F., CHOU, Y. T. & SAIBEL, E. A. 1957 *Trans. A.S.M.E.* **79**, 494.
PATRAT, J. 1975 *J. Méc.* **14**, 505.
SAVAGE, S. B. 1964 *J. Appl. Mech.* **31**, 594.
SCHLICHTING, H. 1934 *Z. Angew. Math. Mech.* **14**, 368.
SCHLICHTING, H. 1960 *Boundary Layer Theory.* McGraw Hill.
THOMAN, D. C. & SZEWCZYK, A. A. 1969 *Phys. Fluids Suppl.* **12**, II 76.
VAN DE VOOREN, A. I. & DIJKSTRA, D. 1970 *J. Engng Math.* **4**, 9.
WANG, Y. L. & LONGWELL, P. A. 1964 *A.I.Ch.E. J.* **10**, 323.
WILSON, S. D. R. 1971 *J. Fluid Mech.* **46**, 787.
WILSON, S. D. R. 1972 *Appl. Sci. Res.* **25**, 349.
WOODS, L. C. 1954 *Aero. Quart.* **5**, 176.
WOOLARD, H. W. 1957 *J. Appl. Mech.* **24**, 9.